Journal of Zhejiang University-SCIENCE A (Applied Physics & Engineering)
ISSN 1673-565X (Print); ISSN 1862-1775 (Online)
www.jzus.zju.edu.cn; www.springerlink.com
E-mail: jzus@zju.edu.cn

Correspondence:

Simulation and experiment of a remotely operated underwater vehicle with cavitation jet technology*#

Jing-ke HU[1,2], Zhe-ming TONG[†‡1,2], Jia-ge XIN[2], Can-jun YANG[1,2]
[1]*State Key Laboratory of Fluid Power and Mechatronic Systems, Zhejiang University, Hangzhou 310027, China*
[2]*School of Mechanical Engineering, Zhejiang University, Hangzhou 310027, China*
[†]E-mail: tzm@zju.edu.cn

https://doi.org/10.1631/jzus.A1900356

1 Introduction

Fouling is the attachment and development of unwanted material on artificial surfaces immersed in seawater (Hachicha et al., 2019). The existence of fouling material leads to many economic and ecological problems in the seabed environment. Over the last 10 years, at least 30 bridges have collapsed in China because of the increase of biofouling thickness. It is important to do regular checks on bridges. An underwater check is now a common method throughout the world. Frogmen will dive underwater with tools to carry out the check. However, this method is slow, expensive, and dangerous.

Cavitation jet cleaning technology is a new underwater method in which cavitation is introduced in the water jet technology (Yamaguchi and Shimizu, 1987; Biçer and Sou, 2016; Cheng et al., 2018). A large number of cavitation bubbles are produced by controlling the pressure, velocity of flow, and other parameters when water passes through the cavitation nozzle. The micro jet impact of 140–170 MPa caused by the collapse of cavitation bubbles in the cleaning surface area is used to clean target surface deposits and dirt (Duraiselvam et al., 2006; Marcon et al., 2016). Compared with other cleaning technologies, it is efficient, energy-saving, environmentally friendly, and safe.

Remotely operated vehicles (ROVs) are essential tools for providing safe access underwater (Goheen and Jefferys, 1990; García-Valdovinos et al., 2014; Khojasteh and Kamali, 2017). In this study, underwater ROV is used as the platform to realize the cleaning of underwater structures based on cavitation jet cleaning technology. The principle of hydrodynamic cavitation is given in Method S1.

2 Numerical simulation of cavitation jet

2.1 Numerical simulation of water nozzle

Computational fluid dynamics (CFD) is a technique for solving various fluid-conservative control differential equations using a computer (Ji et al., 2017; Zhang et al., 2018; Chen et al., 2019; Cheng et al., 2019; Tong et al., 2019a, 2019b). Given the formation conditions and requirements of the cavitation jet, the structure of the nozzle is shown in Fig. 1. The control parameters are throttle diameter d, outlet length L, outlet diameter D, and inlet pressure P. P is the average pressure in the x direction of the inlet cross section. Different blocked things have different surface adhesion, and the proper control parameters

‡ Corresponding author
* Project supported by the National Natural Science Foundation of China (No. 51708493), the National Key R&D Program of China (No. 2018YFB0606105), the Zhejiang Provincial Natural Science Foundation of China (No. LR19E050002), the Key R&D Program of Zhejiang Province (Nos. 2018C01020 and 2018C01060), and the Youth Funds of the State Key Laboratory of Fluid Power and Mechatronic Systems (No. SKLoFP_QN_1804), China
# Electronic supplementary materials: The online version of this article (https://doi.org/10.1631/jzus.A1900356) contains supplementary materials, which are available to authorized users
ORCID: Zhe-ming TONG, https://orcid.org/0000-0003-1129-7439

P-*d*-*L*-*D* are selected to quickly and efficiently clean things that are covered at the bottom of the hole.

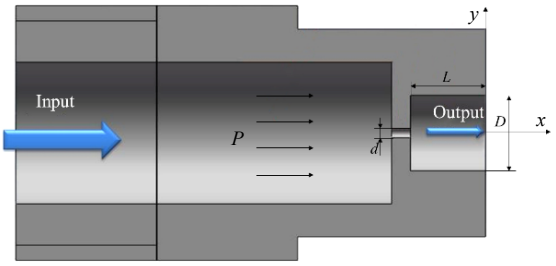

Fig. 1 Nozzle structure with geometric parameters *P*, *d*, *L*, and *D*

2.1.1 Mathematical model and governing equation

1. Continuity equation

$$\frac{\partial}{\partial t}\int_V \alpha_i\rho_i\chi \mathrm{d}V+\oint_A \alpha_i\rho_i\chi(v_i-v_\mathrm{g})\cdot \mathrm{d}a =\int_V\sum_{j\neq i}(m_{ij}-m_{ji})\chi \mathrm{d}V+\int_V S_i^\alpha \mathrm{d}V, \tag{1}$$

where α_i is the volume fraction of phase i, ρ_i is the density of phase i, χ is the cavitation rate, v_i is the velocity of phase i, v_g is the mesh velocity, m_{ij} is the mass transferred from phase j to phase i, m_{ji} is the mass transferred from phase i to phase j, and S_i^α is the source term of phase mass. t is the time, V is the volume, A is the surface area, and a is the acceleration.

In addition, the volume fraction satisfies

$$\sum_i \alpha_i=1. \tag{2}$$

2. Momentum equation

$$\begin{aligned}\frac{\partial}{\partial t}\int_V \alpha_i\rho_i\chi \mathrm{d}V+\oint_A \alpha_i\rho_i\chi v_i\otimes(v_i-v_\mathrm{g})\cdot \mathrm{d}a&=-\int_V \alpha_i\chi\nabla p\mathrm{d}V+\int_V \alpha_i\rho_i\chi g\mathrm{d}V\\&+\oint_A[\alpha_i(\tau_i+\tau_i^\mathrm{t})]\chi\cdot \mathrm{d}a+\int_V M_i\chi \mathrm{d}V+\int_V(F_\mathrm{int})_i\chi \mathrm{d}V\\&+\int_V S_i^v\mathrm{d}V+\int_V\sum(n_{ij}v_j-n_{ji}v_i)\chi \mathrm{d}V,\end{aligned} \tag{3}$$

where p is the pressure, which is assumed to be equal in two phases. g is the gravity acceleration. τ_i and τ_i^t are the molecular stress and turbulent stress, respectively. $(F_\mathrm{int})_i$ represents the internal force. S_i^v is the momentum source term of the phase. n_{ij} is the mass transfer rate from phase j to phase i. n_{ji} is the mass transfer rate from phase i to phase j. M_i is the momentum transfer between phases per unit volume, which represents the force of the interaction between phases:

$$\sum_i M_i=0. \tag{4}$$

2.1.2 Numerical analysis of water nozzle

ANSYS Fluent is used for modeling, meshing, and CFD simulation. As for the nozzle with the same structure size, the inlet pressure P is changed, and the simulation results are as follows. At the same time, the inlet pressure P is controlled unchanged, and by changing the nozzle parameters d, D, and L, the method of cross control variables is used for simulation. The mesh size of the nozzle is 1 120 000 elements. The simulation analysis controls different parameters as variables.

The inlet pressure is the direct cause of jet formation. The nozzle with throat diameter d=2 mm and d:D:L=1:8:8 is selected for the simulation. The pressure at the outlet basin is atmospheric pressure. The inlet pressure P is adjusted to 10 MPa, 15 MPa, 20 MPa, 25 MPa, and 30 MPa, respectively. Fig. 2a is the turbulent kinetic energy (TKE) diagram of the nozzle when P=30 MPa. The contour of TKE shows that after the jet flows from the outlet, the state of the jet is first maintained in a bundle within a certain distance, then gradually diffuses and decelerates, and finally annihilates in still water. When the jet impinges on the target, the impact effect can be affected by adjusting the energy of the jet at different target distances.

Changing the P value means a change in the size of jet carrying energy, so under the same throat diameter, the higher the pressure, the higher the speed. However, when the difference in pressure value is constant, the difference in speed increases as the pressure increases. It can be predicted that when the

pressure height reaches a certain value, the difference of the speed will be reduced to a relatively small value, that is, the speed of the pressure again increases hardly any further.

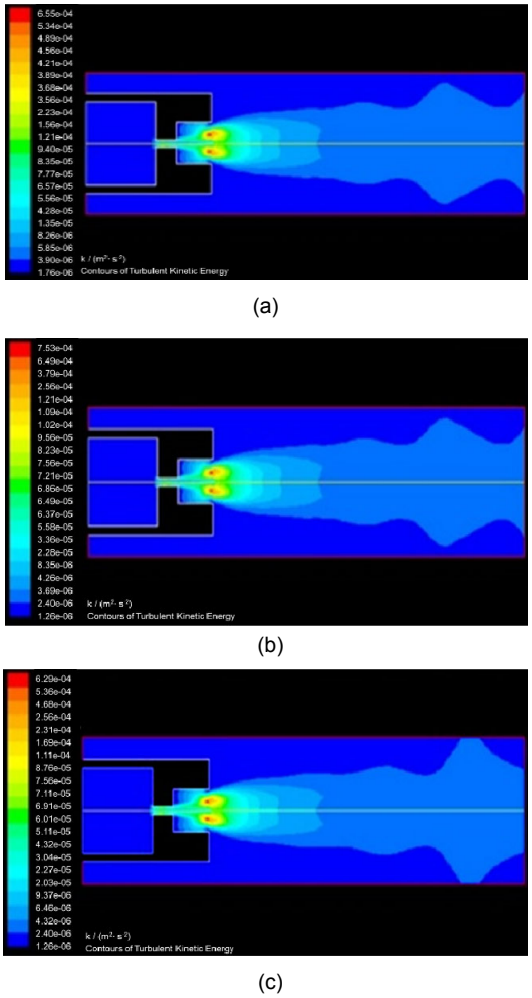

Fig. 2 Contours of turbulent kinetic energy (TKE) of the nozzle under different parameters: (a) *D*=16 mm, *L*=16 mm, *P*=30 MPa; (b) *D*=14 mm, *L*=18 mm, *P*=30 MPa; (c) *D*=14 mm, *L*=16 mm, *P*=30 MPa

The shape of the nozzle outlet is determined by the outlet diameter D and the outlet length L. These are important parameters that affect the flow pattern of the nozzle jet. Suitable parameters can improve the efficiency of the nozzle. The control inlet pressure P is constant, and the simulation conditions are: d=2 mm, P=30 MPa. The length L of the outlet is unchanged, and the diameter D of the outlet is changed to 12, 14, 16, 18 mm, respectively. Fig. 2b is the contour of TKE of the nozzle with D=14 mm when L=18 mm. In the range where the jet does not leave the nozzle, the larger the D value, the higher the exit velocity value. In the case where the value of D is larger, the length of the jet high-speed sustaining section is longer. The jet is maintained at a high TKE for a long period. The longer the high TKE segment, the longer the jet-bundling state and the more jet energy is retained, which is beneficial to the jet in improving the erosion effect. Therefore, the speed maintenance characteristics at D=18 mm are superior to those of the other groups.

When the outlet diameter D is constant and the outlet length L is changed, the TKE diagram of the working condition parameters of the outlet diameter D=14 mm and L=16 mm is shown in Fig. 2c. The length L of the exit has little effect on the speed, but the length of the high-speed sustaining section at L=16 mm is longer and the jet is in a bundled state for a longer period of time, which is consistent with the aforementioned analysis.

Based on the analysis of the above exit shape, the parameter ratio of d:D:L=1:8:8 is selected as the parameter ratio of nozzle processing. When the inlet pressure P=30 MPa, throttle diameter d=2 mm, outlet length L=16 mm, and outlet diameter D=16 mm, the underwater nozzle has the highest cleaning efficiency and can meet the cleaning requirements.

2.2 Soil case simulation for ROV jet simulation analysis

A soil case is selected for ROV jet simulation analysis. Specific parameters are shown in Table 1.

Table 1 Soil case parameter

Parameter	Value
Shear stress (kPa)	2
Boundary pressure of Destruction faces, F_{cr} (MPa)	0.065
Soil particle diameter, d_{60} (mm)	0.22
Density, ρ (kg/m^3)	1950
Particle size (Sauter mean diameter) (mm)	0.2

2.2.1 Numerical analysis of the soil case

Fig. 3 shows the geometric model simulating the ground breaking of the jet in a still water body, including the nozzle, the mud-water interface, and the sediment. The whole model is a 3D cuboid model

with a length of 1.5 m, a width of 0.6 m, and a height of 0.6 m, of which the water body calculation domain is 0.5 m high and the sediment calculation domain is 1 m. The meshing adopts the multi-faceted trolled at 1 cm, the minimum mesh is 2 mm, and the total number of generated meshes is about 850 000 elements. Fig. 4 shows a local mesh refinement of the ROV jet water and mud interface is carried out in order to obtain more accurate results.

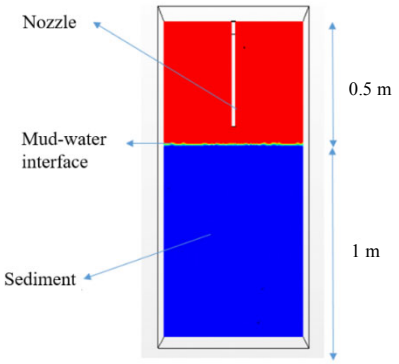

Fig. 3 Geometric model of the ROV jet simulation

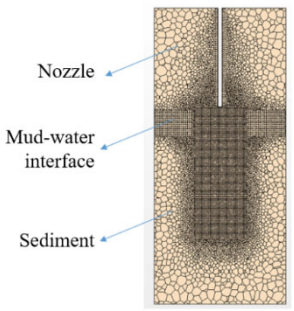

Fig. 4 Meshes of the ROV jet simulation

2.2.2 Simulation results

The parameters of the ROV nozzle jet are complicated, so the nozzle model is simplified. The simulation assumes that the ROV underwater robot has better self-stability in the jet, and the effect on the result is negligible.

1. Influence of jet target distance on jet effect

The target distance is the distance of the ROV nozzle from the underwater mud. We set the injection flow rate Q=0.8 L/s, and analyzed the scour depth of different injection target distances and the optimal jet target distance.

Data in Table 2 are obtained by integrating simulation results of different shooting targets' volume fractions of water in Fig. 5. The results show that the scour depth decreases with the increase of jet target distance.

Table 2 Simulation results of different target distances

Working condition	Jet target distance (mm)	Scour depth (mm)
a	130	22.2
b	90	46.8
c	50	73.5
d	10	129.8

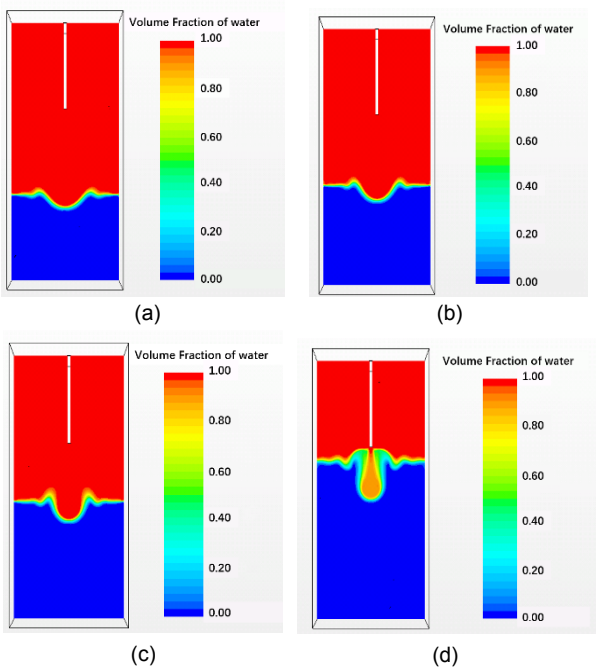

Fig. 5 Simulation results of volume fraction of water at different shooting distances in working conditions a–d of Table 2

2. Influence of jet flow rate on jet effect

We fixed the injection target distance, and analyzed the scour depth of different injection flows and the optimal injection flow.

The simulation results of different injection flow's volume fractions of water in Fig. 6 are integrated to obtain Table 3. According to the simulation results, it can be clearly observed that the scour depth increases with the increase of jet flow. When the injection flow reaches a certain value, the soil scour depth increases slowly. However, in practice, the ROV has limited self-stability and may reach the performance limit much earlier.

3 Cavitation jet experiment

To verify the cavitation effect and cleaning effect of underwater and water nozzles, several experiments were carried out in the robot design and manufacturing process.

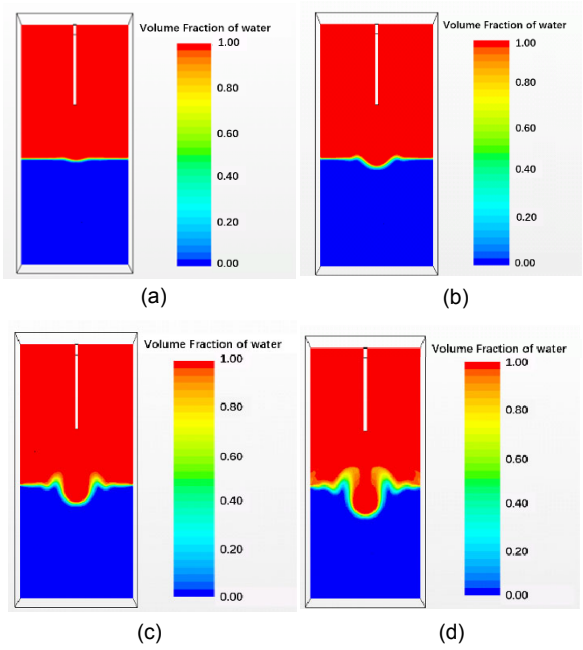

Fig. 6 Simulation results of volume fraction of water at different jet flow rate in working conditions a–d of Table 3

Table 3 Simulation results for different jet flows

Working condition	Scour flow (L/s)	Scour depth (mm)
a	0.2	20.4
b	0.4	48.2
c	0.6	80.8
d	0.8	129.8

3.1 Experimental

The overall layout is shown in Fig. 7. The test system is divided into a test water tank (100 mm× 100 mm×150 mm), an ROV cavitation cleaning device, an experimental attachment surface, and barnacles. The underwater camera is FUJIFILM X-T20 15-45 with a resolution of 24.3 million pixels.

Barnacle is a common, hard, and highly adherent organism that is a common marine cleaning object. We conducted a rattan pot sampling at the seaside in Zhoushan, China, and selected four clusters of barnacles of similar size and shape as the objects of scour. In order to verify the cleaning effect of the ROV cavitation cleaning device on the marine organisms in the laboratory, we applied four clusters of barnacles to the attachment surface with the same angle of super glue, as shown in Fig. 8, to simulate the marine life attached to the pipeline of the offshore oil platform.

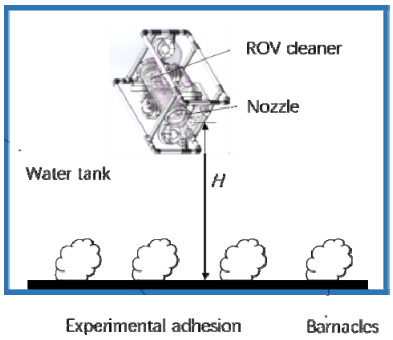

Fig. 7 Overall layout of the experimental setup (*H* is the distance between ROV and barnacles)

Fig. 8 A barnacle attached to a surface

According to the optimized value obtained by the numerical simulation in Section 2.1.2, the working pressure is adjusted to P=30 MPa, and nozzles of d=2 mm, D=16 mm, and L=16 mm are used. The four clusters of barnacles are cavitation cleaned by controlling the distance H of the ROV from the bottom of the water tank by 10 mm, 30 mm, 60 mm, and 100 mm, respectively, and the flushing time is 60 s.

3.2 Results and discussion

Fig. 9 shows the residue of the attached plate after cavitation cleaning for different values of H. By analyzing the experimental results, the following conclusions can be drawn:

1. When H=10 mm, the flushing effect is the best. The flushing effect at H=30 mm is only slightly worse than that at H=10 mm. When the distance between

ROV and barnacles (H=100 mm) is far away from the nozzle, the flushing depth is shallow, so the flushing effect is poor.

2. As with the conclusion of Section 2.2.2, it can be clearly seen that the jet depth decreases as the thrust target distance increases. However, when the pressure is constant and the distance is too close, the erosion intensity will be weakened by the excessive resistance when hitting the sea creatures.

3. The designed cavitation nozzle is capable of crushing most of the jacket sea creature samples, indicating that it has the ability to clean out most of the jacket sea creatures.

4. The actual cleaning effect of the cavitation cleaning device is similar to the expected one. The lower sea creatures are crushed to disengage the upper sea creatures.

5. The efficiency of the cleaning is related to the structure of the sea creature and the direction of the jet. At present, the cleaning mechanism is a simple two-nozzle fixed-direction jet, which is the place where the cleaning mechanism needs to be optimized after further testing.

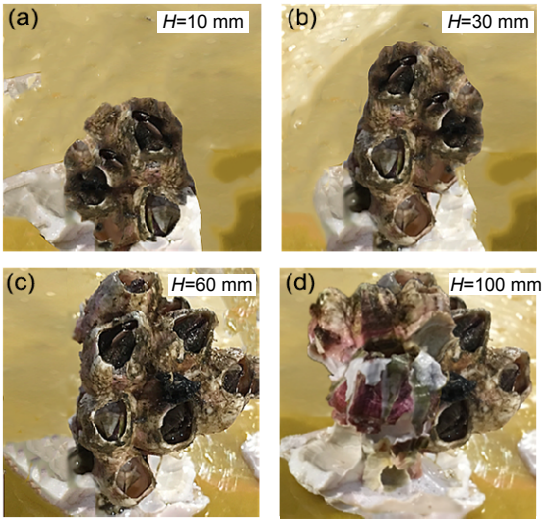

Fig. 9 Residue of the attached plate after cavitation cleaning in the case of H=10 mm (a), H=30 mm (b), H=60 mm (c), and H=100 mm (d)

4 Conclusions

In this paper, an ROV with cavitation jet technology is developed as the platform to realize the cleaning of underwater structures. Based on simulation parameters and multiple experimental results, it is determined that when the inlet pressure P=30 MPa, orifice diameter d=2 mm, outlet length L=16 mm, and outlet diameter D=16 mm, the underwater nozzle has a satisfactory cleaning efficiency that meets the cleaning requirements. At the same time, the further the ROV nozzle is from the mud under the water, the shallower the scour depth is. CFD simulations are conducted to verify the underwater jet cleaning model under the influence of different states and different parameters. We verified the ROV's cleaning effect on marine organisms in the laboratory, and found that the designed cavitation nozzle is capable of crushing most of the jacket sea creature samples.

Contributors

Jing-ke HU conducted the experiment. Jing-ke HU, Zhe-ming TONG, and Jia-ge XIN processed the corresponding data. Jing-ke HU and Zhe-ming TONG wrote the first draft of the manuscript. Zhe-ming TONG, Jia-ge XIN, and Can-jun YANG revised and edited the final version.

Conflict of interest

Jing-ke HU, Zhe-ming TONG, Jia-ge XIN, and Can-jun YANG declare that they have no conflict of interest.

References

Biçer B, Sou A, 2016. Application of the improved cavitation model to turbulent cavitating flow in fuel injector nozzle. *Applied Mathematical Modelling*, 40(7-8):4712-4726. https://doi.org/10.1016/j.apm.2015.11.049

Chen YJ, Tong ZM, Wu WT, et al., 2019. Achieving natural ventilation potential in practice: control schemes and levels of automation. *Applied Energy*, 235:1141-1152. https://doi.org/10.1016/j.apenergy.2018.11.016

Cheng F, Ji WX, Qian CH, et al., 2018. Cavitation bubbles dynamics and cavitation erosion in water jet. *Results in Physics*, 9:1585-1593. https://doi.org/10.1016/j.rinp.2018.05.002

Cheng ZW, Tong SG, Tong ZM, 2019. Bi-directional nozzle control of multistage radial-inflow turbine for optimal part-load operation of compressed air energy storage. *Energy Conversion and Management*, 181:485-500. https://doi.org/10.1016/j.enconman.2018.12.014

Duraiselvam M, Galun R, Siegmann S, et al., 2006. Liquid impact erosion characteristics of martensitic stainless steel laser clad with Ni-based intermetallic composites and matrix composites. *Wear*, 261(10):1140-1149. https://doi.org/10.1016/j.wear.2006.03.024

García-Valdovinos LG, Salgado-Jiménez T, Bandala-Sánchez M, et al., 2014. Modelling, design and robust control of a remotely operated underwater vehicle. *International*

Journal of Advanced Robotic Systems, 11(1):1. https://doi.org/10.5772/56810

Goheen KR, Jefferys ER, 1990. Multivariable self-tuning autopilots for autonomous and remotely operated underwater vehicles. *IEEE Journal of Oceanic Engineering*, 15(3):144-151. https://doi.org/10.1109/48.107142

Hachicha S, Zaoui C, Dallagi H, et al., 2019. Innovative design of an underwater cleaning robot with a two arm manipulator for hull cleaning. *Ocean Engineering*, 181:303-313. https://doi.org/10.1016/j.oceaneng.2019.03.044

Ji SM, Ge JQ, Tan DP, 2017. Wall contact effects of particle-wall collision process in a two-phase particle fluid. *Journal of Zhejiang University-SCIENCE A (Applied Physics & Engineering)*, 18(12):958-973. https://doi.org/10.1631/jzus.A1700039

Khojasteh D, Kamali R, 2017. Design and dynamic study of a ROV with application to oil and gas industries of Persian gulf. *Ocean Engineering*, 136:18-30. https://doi.org/10.1016/j.oceaneng.2017.03.014

Marcon A, Melkote SN, Castle J, et al., 2016. Effect of jet velocity in co-flow water cavitation jet peening. *Wear*, 360-361:38-50. https://doi.org/10.1016/j.wear.2016.03.027

Tong ZM, Li Y, Westerdahl D, et al., 2019a. Exploring the effects of ventilation practices in mitigating in-vehicle exposure to traffic-related air pollutants in China. *Environment International*, 127:773-784. https://doi.org/10.1016/j.envint.2019.03.023

Tong ZM, Cheng ZW, Tong SG, 2019b. Preliminary design of multistage radial turbines based on rotor loss characteristics under variable operating conditions. *Energies*, 12(13):2550. https://doi.org/10.3390/en12132550

Yamaguchi A, Shimizu S, 1987. Erosion due to impingement of cavitating jet. *Journal of Fluids Engineering*, 109(4):442-447. https://doi.org/10.1115/1.3242686

Zhang JH, Wang D, Xu B, et al., 2018. Experimental and numerical investigation of flow forces in a seat valve using a damping sleeve with orifices. *Journal of Zhejiang University-SCIENCE A (Applied Physics & Engineering)*, 19(6):417-430. https://doi.org/10.1631/jzus.A1700164

List of electronic supplemental material

Method S1 Principle of hydrodynamic cavitation

中文概要

题　目：基于空化喷射技术的水下机器人射流清洗仿真与实验

目　的：污染物质的存在会引起海底环境中的许多经济和生态问题。本文以遥控无人潜水器（ROV）为基础承载平台，实现基于空化喷射清洗技术的水下结构表面附着物清洗。

创新点：将空化射流清洗技术与 ROV 结合，并利用空化泡在清洗表面区域溃灭产生的微射流冲击，以达到清理水下表面附着物和污垢层的目的。

方　法：1. 通过计算流体动力学（CFD）仿真与实验，针对 ROV 水下喷射模型，在不同状态和不同参数下对水下射流的规律进行测试与比较。2. 实验对比验证在不同喷射距离下所设计的空化射流清洗装置清理海底生物的能力。

结　论：1. 当入口压力 P=30 MPa，孔径 d=2 mm，出口长度 L=16 mm 和出口直径 D=16 mm 时，水下喷嘴具有更高的清洁度和清洁效率，可以满足清洁要求。2. ROV 喷嘴离水下泥浆越远，冲刷深度越浅。3. 所设计的 ROV 空化喷射清洁装置与目标的距离越近，清洗强度越高；然而，当压力恒定且距离太近时，过度阻力会削弱冲洗强度。

关键词：水下喷射；ROV；空化喷射清洁；喷嘴结构